Composites Part B 166 (2019) 352–360

Contents lists available at ScienceDirect

Composites Part B

journal homepage: www.elsevier.com/locate/compositesb

Synergistic icephobic behaviour of swollen nitrile butadiene rubber graphene and/or carbon nanotube composites

L. Valentini[a,*], S. Bittolo Bon[a], N.M. Pugno[b,c,d], M. Hernandez Santana[e], M.A. Lopez-Manchado[e], G. Giorgi[f,**]

[a] Civil and Environmental Engineering Department, University of Perugia, UdR INSTM, Strada di Pentima 4, 05100, Terni, Italy
[b] Laboratory of Bio-Inspired and Graphene Nanomechanics, Department of Civil, Environmental and Mechanical Engineering, University of Trento, Via Mesiano 77, 38123, Trento, Italy
[c] School of Engineering and Materials Science, Queen Mary University of London, Mile End Road, London, E1 4NS, United Kingdom
[d] Ket Labs, Edoardo Amaldi Foundation, Italian Space Agency, Via del Politecnico snc, 00133, Rome, Italy
[e] Instituto de Ciencia y Tecnología de Polímeros, ICTP-CSIC, Juan de la Cierva, 3, 28006, Madrid, Spain
[f] Civil and Environmental Engineering Department, University of Perugia, Via G. Duranti, 93, I-06125, Perugia, Italy

ARTICLE INFO

Keywords:
Nano-structures
Mechanical properties
Computational modelling
Mechanical testing

ABSTRACT

Spontaneous change of adhesion of solidifying liquid on surfaces is of significant importance in materials technology where it finds applications such as anti-icing components operating in extreme environments like those of seals. In this work, nitrile butadiene rubber (NBR) composites reinforced with graphene, carbon nanotubes, and a mix of them after immersion in several fluids, experienced both a swelling and a reduction of the cross-link density that reduces ice adhesion, being this effect more evident for graphene containing samples. These results have been rationalized via a first principles atomistic modellization of interfaces formed by ice water of increasing thickness and graphene and scaling laws from fracture mechanics, revealing a clear synergy between swelling and nanocarbon phase in the icephobic nature of the composite, dictated by a competition between elastic modulus and adsorption energy. These findings could find an upscale in component validation readily applied to different areas where de-icing demands handling of large amount of environmental harmful agents.

1. Introduction

Elastomers are commonly considered the workhorses of the industrial and automotive components because of their good resistance to lubricants and greases and their relatively low cost. Nowadays, there is a continue need to develop high performance composites for use in the exploration and operational drilling applications in extreme locations where the extreme conditions such icing problems become hazardous, limiting the extraction activities unless reliable solutions are found. In transportation, bearing seals mounted on aircraft components are subjected to icing problems that require a solution. More in general, the removal of accreted ice remains an expensive daily and industrially concern across the globe [1,2].

Different chemical and physical methods have been developed to remove ice once formed, e.g. heaters, hot water/glycol mixtures, vibrators, pneumatic boots on aircrafts, or to prevent the water wettability, e.g. nanostructured ice-phobic coatings [3–9].

In general, the adhesion of ice on stiff substrate without interfacial defects are hard be separated. However, if one of the solids is deformable, then they can be separated imposing a differential deformation. Kim et al. [10] found that polymeric films of low modulus and low surface energy do promote easy release and demonstrated that the critical shear stress of fracture decreases with the shear modulus of an elastomeric surface. Thus, when ice adhered to a low cross-link elastomer experiences a shear stress, the ice detaches from the ice-elastomer interface at low applied loads [5]. For elastomers, it is known that the modulus is related to the cross-link density that can be calculated by the well-known Flory formula [11]; durable organogel anti-icing material via swelling cross-linked poly(dimethylsiloxane) with liquid paraffin was reported [8] while Golovin et al. [12] recently predicted the icephobicity of different types of polymers by filling a polymer with oil. They optimized the polymer/plasticizer (i.e. oil)

* Corresponding author.
** Corresponding author.
E-mail addresses: luca.valentini@unipg.it (L. Valentini), giacomo.giorgi@unipg.it (G. Giorgi).

https://doi.org/10.1016/j.compositesb.2018.11.095
Received 4 May 2018; Received in revised form 31 October 2018; Accepted 25 November 2018
Available online 28 November 2018
1359-8368/

Table 1
Recipes of the rubber compounds (indicated in phr: parts per hundred of rubber).

sample	NBR	ZnO	Stearic acid	MBT - (2-Mercaptobenzothiazole)	S	CNT	GNPs
NBR-0	100	5	1.5	1.5	1.5	0.0	0.0
NBR-1	100	5	1.5	1.5	1.5	0.0	5.0
NBR-2	100	5	1.5	1.5	1.5	5.0	0.0
NBR-3	100	5	1.5	1.5	1.5	2.5	2.5

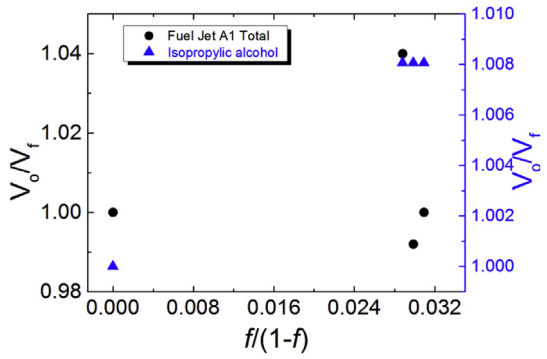

Fig. 1. Kraus plot after swelling test on NBR containing GNPs/CNTs fillers.

combinations to obtain low ice adhesion and good mechanical durability.

Recently Park et al. [13,14] demonstrated that the hybrid filler provided significant enhancement of mechanical properties, such as flexural strength, flexural modulus, and fracture toughness. In particular, the epoxy composite containing graphene hybrid exhibited a stronger mechanical behaviour [13]. Here we are interested in investigating the physical properties and swelling of neat nitrile butadiene rubber (NBR) and respective graphene and/or carbon nanotubes (CNTs) composites and understanding their surface adhesion properties with specific attention to ice. Concerning graphene, its interaction with water/ice is an extremely broad and deeply investigated topic [15] for which no conclusive homogeneous results have been provided so far. On the theoretical side, many aspects of the interaction mechanisms have been investigated such as the role of the substrate [16], *i.e.* the different behaviour in terms of structural and electronic properties for water layers and ice interacting with graphene and with graphene on a substrate. Focusing on the adsorption mechanism of water clusters and ice dimers on graphene, Leenarts et al. [17] found a hydrophobic and icephobic behaviour of graphene with an adsorption energy that increases as the cluster size increases, with a convergence limit of ~13 meV per molecule, while ice dimers result slightly stronger bound to graphene. As widely reported, the adsorption energy of the water and ice water molecule is highly influenced by its orientation and not secondarily its calculation is affected by the adopted theoretical scheme to describe the mechanism [18]. The different outcomes associated with different experimental conditions and theoretical setup somehow indicate that pairing the two approaches is mandatory in order to obtain meaningful comparisons [15], *i.e.* the choice of the theoretical setup (models and level of calculation) highly depends on the experimental phenomena to be modelled.

In the present paper we prepare graphene and/or CNTs based rubber composites and measure their ice adhesion after fluid susceptibility tests. First principles atomistic modellization of interfaces formed by ice water of increasing thickness and graphene show a clear icephobic nature of graphene that linearly increases with the thickness of ice. The predictive design and behaviour of such composites in extreme environment would be applicable to the automotive and aviation sectors, where the demand for multifunctional rubbers is increasing.

2. Experimental details

An Acrylonitrile Butadiene rubber (NBR) under the trade name Krynac 2850F (acrylonitrile content: 27.5 wt%, Mooney viscosity M_L (1 + 4) 100 °C 48 and a density of 0.97 g/cm^3) was used as rubber matrix. Multi-walled carbon nanotubes were kindly supplied by Nanocyl S.A. under the trade name Nanocyl NC7000. Graphene nanoplatelets (GNPs) were kindly supplied by NANESA (G3Nan average thickness of 9 nm ≈ 25 layers, average lateral particle size 15 μm).

Rubber compounds were prepared in an open two-roll mill at room temperature. The rotors operated at a speed ratio of 1:1.4. The vulcanization ingredients were sequentially added to the rubber before to the incorporation of the filler and sulphur. The recipes of the compounds are described in Table 1. Vulcanizing conditions (temperature and time) were previously determined by a Monsanto Moving Die Rheometer MDR 2000E. Rubber compounds were then vulcanized at 160 °C in a thermofluid heated press. The vulcanization time of the samples corresponds to the optimum cure time t_{90} derived from the curing curves of the MDR 2000E. The filler volume fraction was calculated from the well-known relationship: $f = (W_f/\rho_f)/(W_f/\rho_f + W_m/\rho_m)$, where W_f is the weight fraction of the filler and W_m is the weight fraction of the matrix, while ρ_f and ρ_m are the densities of the filler (i.e. 1.75 g/cm^3 [19] for CNTs and 1.70 g/cm^3 for GNPs) and the matrix, respectively. For the case of the hybrid filler, i.e. presenting both GNPs and CNTs, the equation was adjusted in order to take into account the presence of both fillers in the matrix volume.

Isopropyl alcohol and Jet A1 Total 20 were used as fluids for immersion. For each fluid, according to the test procedure ASTM D 471, five specimens have been immersed in the appropriate fluid for 70 h at the temperatures of 50 °C and 40 °C for isopropyl alcohol and Jet A1

Table 2
The filler volume fraction content (f) of the respective nanocomposites reported in Table 1 and resulting hardness, elongation at break, tensile strength, modulus (at 50% strain), swelling ratios and liquid volume fraction (Φ_{LIQUID}) before and after liquid immersion. The superscripts (*) and (**) indicate the properties after the immersion in Jet A1 Total 20 and isopropyl alcohol, respectively.

Sample (GNPs/CNTs)	*f*	Hardness (ShA)	Elongation at break (%)	Tensile strength (MPa)	Modulus (MPa)	Swelling	Φ_{LIQUID}
0/0	0	63.5 ± 0.7	498 ± 59	1.62 ± 0.12	0.62 ± 0.02	–	–
0/0(*)		59.0 ± 0.7	317 ± 40	1.26 ± 0.12	0.49 ± 0.02	1.25 ± 0.02	0.402
0/0(**)		61.0 ± 0.7	182 ± 4	0.79 ± 0.02	0.44 ± 0.02	1.24 ± 0.02	0.390
5/0	0.030	65.5 ± 0.7	724 ± 81	3.82 ± 0.41	1.18 ± 0.02	–	–
5/0(*)		59.5 ± 0.7	455 ± 104	2.38 ± 0.29	0.96 ± 0.02	1.24 ± 0.02	0.413
5/0(**)		61.5 ± 0.7	354 ± 12	1.68 ± 0.25	0.79 ± 0.02	1.30 ± 0.02	0.410
0/5	0.028	69.0 ± 0.7	586 ± 25	7.08 ± 0.54	0.79 ± 0.02	–	–
0/5(*)		68.5 ± 0.7	384 ± 43	4.54 ± 0.09	0.69 ± 0.02	1.24 ± 0.02	0.408
0/5(**)		64.5 ± 0.7	306 ± 14	3.74 ± 0.25	0.53 ± 0.02	1.24 ± 0.02	0.409
2.5/2.5	0.028	68.5 ± 0.7	699 ± 63	5.44 ± 0.56	1.03 ± 0.02	–	–
2.5/2.5(*)		62.5 ± 0.7	494 ± 62	3.54 ± 0.24	0.79 ± 0.02	1.25 ± 0.02	0.416
2.5/2.5(**)		63.5 ± 0.7	363 ± 37	2.90 ± 0.09	0.70 ± 0.02	1.25 ± 0.02	0.421

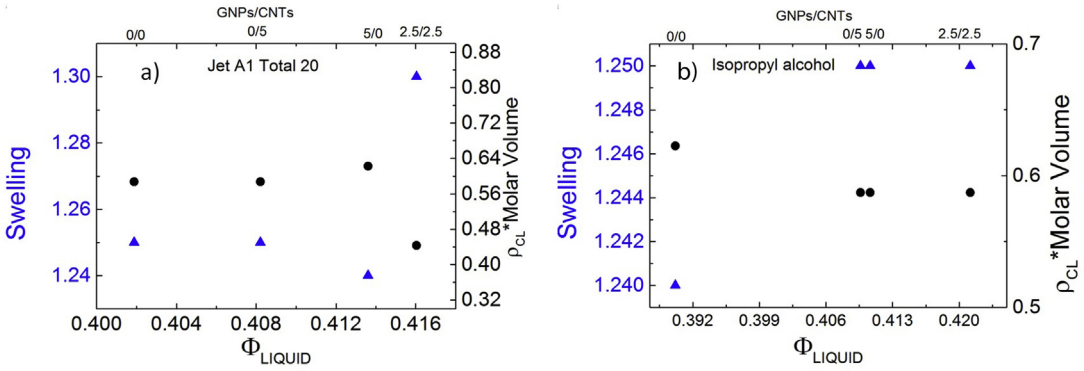

Fig. 2. Swelling and cross-link density reduction of liquid-filled GNPs/CNTs nanocomposites for (a) Jet A1 Total 20 and (b) isopropyl alcohol.

Total 20, respectively. At the end of the required immersion period, the specimens were cooled down to room temperature for 30–60 min, then dipped quickly in acetone at room temperature, and blot lightly with filter paper. Tensile stress-strain properties were measured according to ASTM D 412 specifications, on an Instron dynamometer (Model 4301) at 25 °C. At least three specimens of each sample were tested. The hardness measurements were performed with a durometer according to ASTM D 2240. At least five indentations on each sample were performed.

The swelling studies were performed on a known volume and weight of vulcanized rubber in the form of a rectangular sample that was taken for swelling measurements in immersion liquids. After attaining equilibrium swelling (70 h), its weight was recorded and the volume variation was estimated according to ASTM D 471. Five measurements for each liquid were carried out. The ice adhesion strength was measured using a custom setup, where a force transducer was fixed to a slipping table. Prisms with the dimension of 10 mm × 10 mm × 6 mm were positioned on the sample surface and then filled with water. They were then frozen for 12 h at −20 °C. The shear force was applied at a distance of about 1 mm from the prism-elastomer interface. The measurement was performed at −10 °C. A FTA 1000 Series instrument equipped with a CCD camera was used to measure the ice contact angles on various substrates. Deionized water droplets were dropped onto the rubber surfaces and the contact angle was monitored statically as a function of time. The measurement was carried out on top of a liquid-cooled Peltier cooling plate (TECA Corporation, model LHP-800CP) while purging nitrogen to reduce humidity and thus frost formation on the samples. The obtained values were the average of three measurements, and the typical error in the measurements was ± 4°. The morphologies of the prepared samples were investigated by atomic force microscopy (AFM). AFM images were obtained in tapping mode. Field emission scanning microscopy (FESEM) was performed on the cross section of the samples by means of Zeiss Supra 35.

3. Computational details

Density Functional Theory (DFT) based simulations have been performed by means of a numerical atomic based approach SIESTA code [20,21]. The vdW-DF2 (LMKLL) [22,23] non-local density functional was employed along with the norm–conserving pseudopotentials of the Troullier–Martins (TM) [24] type for the description of the core electrons. The plane wave cut–off was set to 200.0 Ry. The very first step for this kind of analysis was the optimization of graphene and ice structure. For both systems we started from the experimentally reported lattice. For ice in particular we considered as initial guess the hexagonal crystal (I_h) with symmetry $P_{6(3)/mmc}$ ($Z = 4$) at −66 °C [25].

The geometry optimization has led to a structure for graphene characterized by $a = b = 2.506$ Å (821 k-points employed in the Brillouin Zone, BZ), while for ice we got a geometry where $a = b = 4.401$ Å and $c = 7.164$ Å (10 × 10 × 6 Γ-centred sampling of the BZ, corresponding to 338 k-points). As a further validating test, for ice we calculated the Bulk Modulus, finding a value of 8.92 GPa, not far from the experimentally reported data of Mellor (~9.0 GPa) for the bulk modulus of pure polycrystalline ice at T ≪ 0 °C [26].

4. Results and discussion

The cross-link of the filler with the matrix can be estimated from the well-known Kraus relationship [27] that plots (Fig. 1) the ratio of the volume fraction of the swollen rubber (V_0) and swollen filled rubber (V_f), against $f/(1\text{-}f)$ where the slope represents the polymer-filler interaction parameter. For V_0/V_f values higher than 1 this means that during the swelling the matrix separates from the fillers indicating a weak cross linking between the polymer and the filler [27].

The swelling is thus an equilibrium state obtained when the dimensions of the elastomer increase until the concentration of the liquid is uniform throughout the component [28]. This relationship is quantitatively expressed by the Flory-Rehner equation [29]:

$$\rho_{CL} = [\ln(1\text{-}V_r) + V_r + \chi V_r^2]/V[V_r^{1/3}\text{-}0.5V_r] \quad (1)$$

Where V_r is the volume fraction of polymer in a swollen state, χ is the Flory-Huggins interaction parameter between the polymer and the solvent and V is the molar volume of the solvent.

According to the Flory and Rehner theory [29] we calculate the volume fraction of the liquid within the swollen elastomers from the well-known relationship:

$$\Phi_{LIQUID} = (W_{LIQUID}/\rho_{LIQUID})/(W_{LIQUID}/\rho_{LIQUID} + f + W_m/\rho_m), \quad (2)$$

Where W_{LIQUID} is the weight fraction of the liquid calculated from the relative difference of the weights of the sample in its dry and swollen state, f is the volume fraction of the filler and W_m is the weight fraction of the matrix, while ρ_{LIQUID} and ρ_m are the densities of the liquid and polymer matrix, respectively. The results were reported in Table 2. In Fig. 2a and b, we show the decrease of the cross-link density of the three different rubber composites after swelling in different liquids. The mechanical properties reported in Table 2 describe also how a certain amount of liquid reduces the cross-link density and thus, the hardness, tensile strength, elongation at break and modulus of the prepared composites.

In Fig. 3, we present the ice adhesion data for the three different nanocomposites after liquid immersion, where τ^{ice}_{liquid} is the nominal (evaluated as shear force/interface area) adhesion strength of liquid filled sample while $\tau^{ice}_{no\ liquid}$ is the adhesion strength of the un-filled sample. First, we observed the reduction in ice adhesion strength ratio between the swollen and un-swollen composite with the decrease of the cross-link density.

We then investigated the reduction in ice adhesion strength ratio

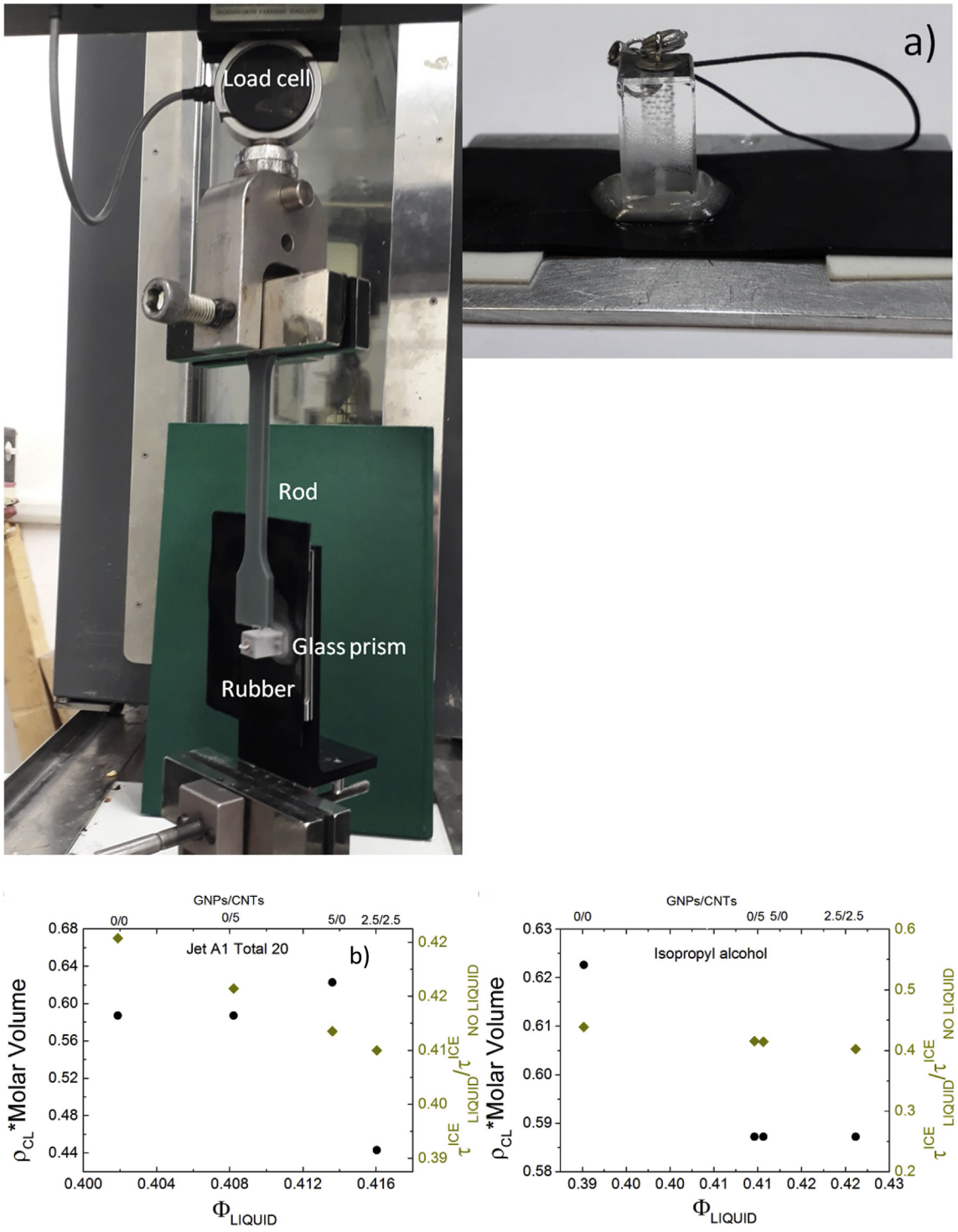

Fig. 3. (a) Measurements of adhesive strength of a glass prism frozen on swollen elastomer. The inset shows the glass prism frozen on elastomer. (b) Measured τ^{ice} for NBR nanocomposites obtained with different GNPs/CNTs combinations as a function of the liquid volume fraction.

between the swollen and un-swollen composite by means of surface characterization of the prepared samples. The values of the contact angle and surface roughness reported in Fig. 4a and b and Table 3, indicate that the higher contact angle values after the fluid treatment is not correlated to the surface topography which is within the experimental error after the fluid immersion and that, in accordance with the study of Jung et al. [30], our results suggest that the hydrophilic surfaces before the treatment (Fig. 4a) may become icephobics (see Table 4).

Moreover, from a deeper investigation of the cross section of the 5/0 sample (Fig. 4c and Supplemenray Material) we observed a confinement of the graphene sheets on the surface. This finding was also confirmed by the enhancement of the surface electrical conductivity with respect to that observed for the bulk resistance (inset of Fig. 4c). We argue that the graphene and ice interface is comparable with that of graphene reinforced rubber and ice. Thus, on the theoretical side it is worth investigating the interface region of the system constituted by graphene and ice, trying to establish a trend in the ice-philic/-phobic

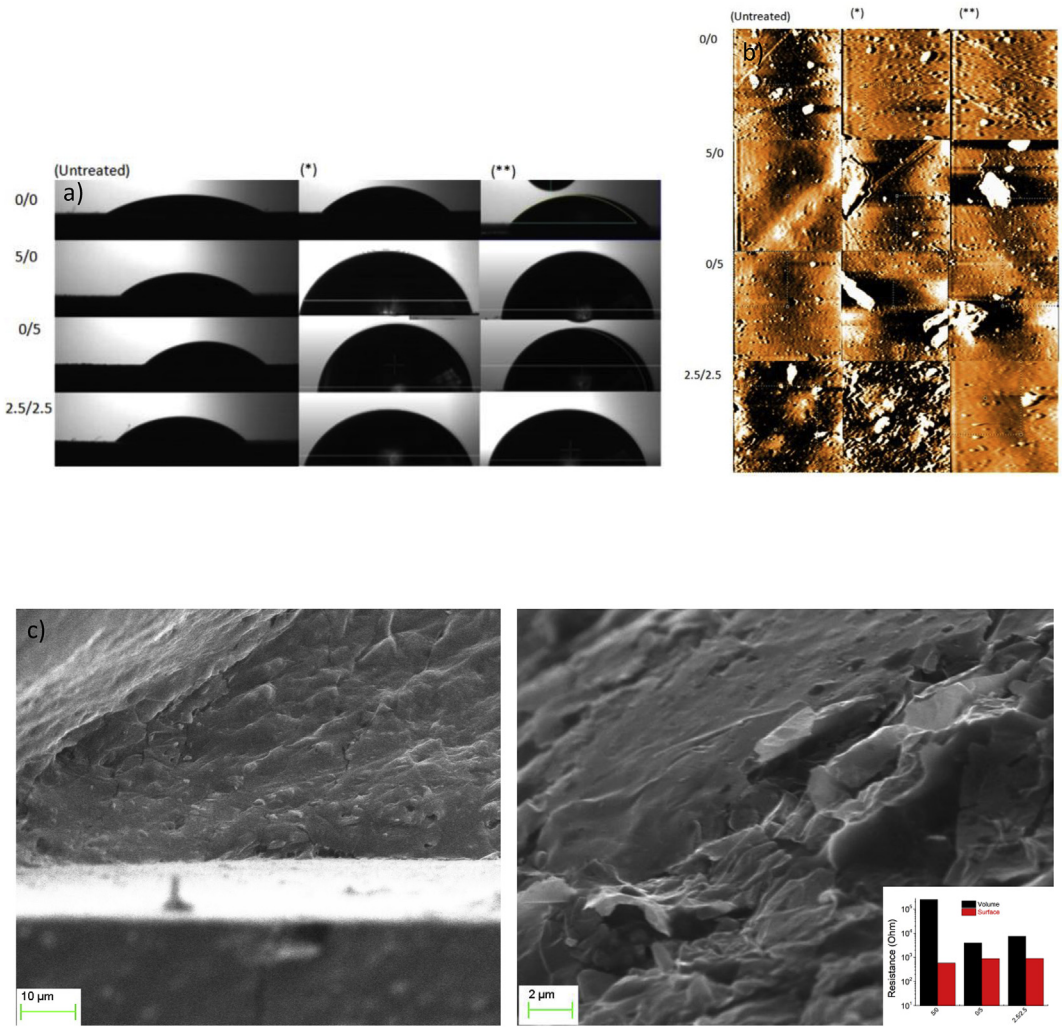

Fig. 4. (a) CCD images of ice on different rubber substrates and (b) corresponding topographical scans (70 μm × 70 μm) by AFM. The superscripts (*) and (**) indicate the properties after the immersion in Jet A1 Total 20 or isopropyl alcohol, respectively. (c) FESEM images at different magnifications of the cross section of the 5/0 nanocomposite. The inset shows the surface and volume electrical resistance values of different rubber compounds.

Table 3
Nanocomposites reported in Table 1 and resulting contact angle and surface roughness before and after liquid immersion. The superscripts (*) and (**) indicate the properties after the immersion in Jet A1 Total 20 and isopropyl alcohol, respectively.

Sample (GNPs/CNTs)	Contact angle (°)	Surface roughness (μm)
0/0	21 ± 4	0.11 ± 0.03
0/0(*)	40 ± 4	0.12 ± 0.02
0/0(**)	45 ± 4	0.12 ± 0.02
5/0	33 ± 4	0.13 ± 0.03
5/0(*)	60 ± 4	0.16 ± 0.06
5/0(**)	73 ± 4	0.12 ± 0.01
0/5	33 ± 4	0.10 ± 0.02
0/5(*)	80 ± 4	0.10 ± 0.02
0/5(**)	78 ± 4	0.14 ± 0.02
2.5/2.5	36 ± 4	0.20 ± 0.08
2.5/2.5(*)	67 ± 4	0.16 ± 0.04
2.5/2.5(**)	73 ± 4	0.14 ± 0.03

nature of graphene.

In order to do it, considering that (*i*) assembling an interface formed by hexagonal cells may result in an unpractical procedure due to the presence of γ angle different from 90°, that (*ii*) in our case *a* and *b* lattice parameters of the two subsystems forming the final interface are noticeably different, a rotation procedure in both cells in order to transform γ angle at 90° (see Fig. 5 for what concerns graphene) will result beneficial to obtain a final interface tetragonal, with the advantage that the so-obtained in plane lattice parameters of graphene and ice have a very small mismatch. Importantly, as we see in the following, such mismatch is not only negligible once the interface is assembled along the [001] direction of ice, but it is also minimal once the interface considered is that formed by [100]-oriented ice and graphene. It is worth mentioning that the same rotation procedure has been successfully applied in interfaces formed by graphene and TiO_2 nanosheets [31].

In details, the new lattice parameters obtained for the tetragonal ice cell are $a = 7.57$, $b = 4.42$, and $c = 7.14$ Å, while those for graphene are $a = 7.51$ and $b = 4.34$ Å, respectively. In this way, at first, we can calculate the (compressive) stress that ice, oriented along the [001] direction [25], experiences once it is deposited on graphene. From our calculations we get $\Delta E = 0.014$ eV (corresponding to the mechanical stress energy) and $\Delta A = 0.866$ Å^2, confirming the negligible stress present at the [001]-oriented ice/graphene interface.

It is important to mention that bulk model of I_h ice has a net dipole moment along *z*. Even if the calculation of its energy does not represent a real issue [32,33], and also considering the *z* direction a natural initial choice in assembling the interface – it is indeed the non-periodic direction for graphene – it becomes quite problematic to assemble an interface whose non-periodic direction contains a dipole. To overcome

Table 4
Adsorption energy per molecule of H_2O (eV/molecule) vs. number of H_2O layers (n = 1–3).

n	Bulk	NSs
1	0.0309	0.0294
2	0.0120	0.0116
3	0.0058	0.0058

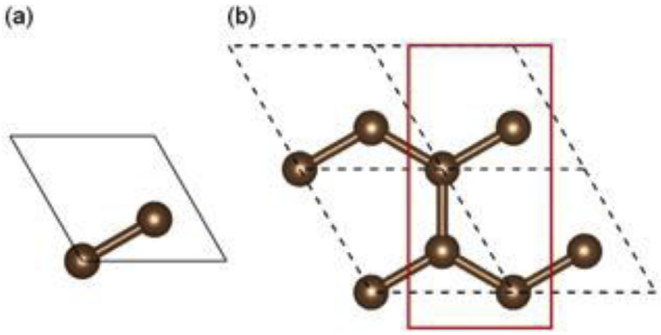

Fig. 5. (a) Unit cell of graphene; (b) 2 × 2 supercell of graphene and (in the red rectangle) the used 4-atoms unit cell (Reproduced with permission from Ref. [31] Copyright © 2014 by John Wiley & Sons, Inc.). (For interpretation of the references to colour in this figure legend, the reader is referred to the Web version of this article.)

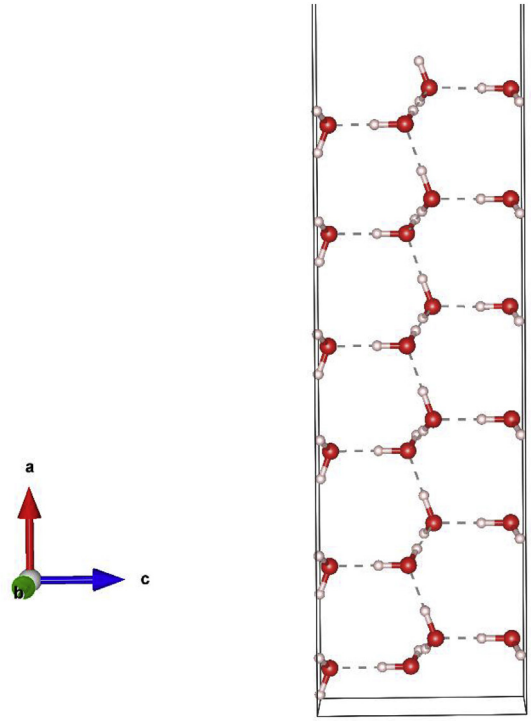

Fig. 6. Optimized structure of a 3-layers slab of ice [100] oriented.

such issue, we then decided to consider *not* the [001] direction, but the non-polar [100] one, where the surface mismatch between the tetragonal ice slab and graphene is still sufficiently small not to give noticeable effects (~3%).

A three layer of such facet is reported in Fig. 6. For such slab, following previous literature [34–36], we similarly calculated the surface energy. To do it we refer to the equation:

$$E_{surf} = \frac{E_{slab} - n \cdot E_{ice}}{2 \cdot S} \quad (3)$$

where E_{slab} is the energy of the slab of ice considered, E_{ice} is the chemical potential of ice water as obtained from the bulk, S (considered twice, since the system is symmetric) is the area of the exposed surface of the slab and n is the number of ice unit in the slab considered (24 in our case). The energy of such surface is 0.54 J/m^2. We tested the energy convergence increasing up to 4 layers of ice the thickness of the slab along x, finding a difference in energy < 0.6%.

To assemble the ice/graphene heterostructure, we have considered three units of ice along the non-periodic direction x, [100], further adding ~20 Å of vacuum on top of ice in order to avoid any possible spurious interactions between replicas of the interface along x. Importantly, the lattice parameters of the interface are the same (optimized) of graphene, since the model here aims to mimic the growth of ice on graphene layers.

Furthermore, due to the asymmetric nature of the interface, we have corrected the dipole present along the [100] direction. We are aware that thicker layers should be used for a more realistic description of such systems: we are similarly aware that for our purpose, *i.e.* to get an atomistic description of phenomena that take place at the very interface, three layers are a sufficient and computationally accessible amount.

The stress energy contribution is mainly mechanical (no chemical) since ice is “one-legged” [37] physisorbed on graphene as shown in Fig. 7, where the optimized structure of the most stable interface ice/graphene is reported.

In details, the closest distance between atoms of the graphene layer and those of ice (H, in this case) is ~2.37 Å, with such atoms lying at the midpoint of a C=C bond (See Fig. 8).

We thus calculate the adsorption energy for the interface corrected for the Basis Set Superposition Error (BSSE) [38]. To do it we have used the equation:

$$E_{ads} = (E_{ice} + E_{graphene}) - E_{interface} \quad (4)$$

From such equation it is clear that the more positive is the adsorption energy, the more stable is the interface.

Recent theoretical and experimental results have shown that according to its dimensionality, 3D bulk or 2D layered ice is characterized by different structures [39–42]. Even if this kind of analysis is out-of-scope of the present paper, it is worth mentioning the small variations in terms of adsorption energy, reported in the following, that appear once we treat ice as bulk (3D) or as a nanosheet (NS) in the formation of the heterostructure with graphene.

In the case of *bulk ice* interfaced with graphene we have to add a term in Eq. (4) to take into account the energy difference between the three layers (3L) keeping ice bulk lattice parameters (7.14 × 4.42 Å^2) and three layers keeping the interface (i.e. those of graphene, 7.51 × 4.34 Å^2) lattice parameters. In this way we obtain an E_{ads} = 0.141 eV. To test the effect of ice thickness *vs* adsorption energy we have reduced the ice amount to two layers (2L) at first and finally to one layer (1L). The adsorption energies in this case result E_{ads} = 0.192 eV (2L) and 0.247 eV (1L), respectively. Such results are in agreement with a power law scaling predicted by fracture mechanics in the form $E_{ads}(n) = E_{ads}(1)/n^x$, where n is the number of ice layer and theoretically x = 0.5 [43] whereas experimentally here $x \cong 0.47$.

Moreover, to consider the layers of ice as NSs we have to add a term in Eq. (4) to take into account the energy difference between the three layers whose in-plane lattice parameters are fully optimized and the three layers keeping the interface (i.e. those of graphene, vide supra) lattice parameters. As in the previous case we tested the same procedure for three different thicknesses of ice, *i.e.* n = 1,2,3. As expected, we obtain values of E_{ads} close for the two approaches but still noticeably different, mainly for thinner layers. In particular, for n = 3 we get E_{ads} = 0.140 eV, for n = 2 E_{ads} = 0.185 eV, and for n = 1 we get E_{ads} = 0.235 eV. Again, such results are in agreement with the previous scaling with $x \cong 0.51$.

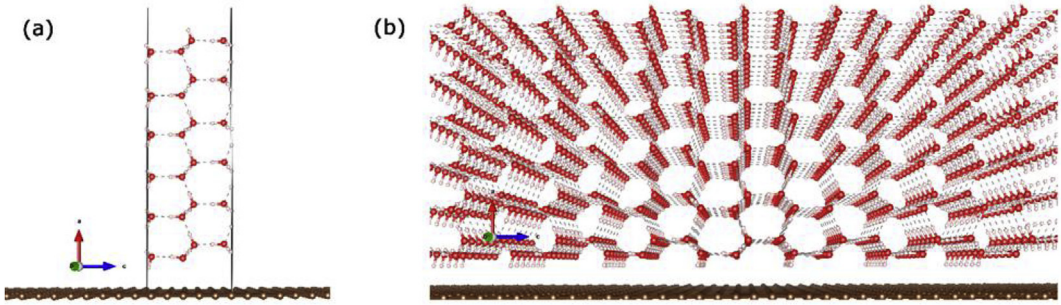

Fig. 7. Lateral views of the supercell of the most stable interface optimized. (a) Unit cell. (b) 5 × 5 supercell (Red: O atoms, white: H atoms, brown: C atoms. Dashed bonds: H-bonds among water molecules). (For interpretation of the references to colour in this figure legend, the reader is referred to the Web version of this article.)

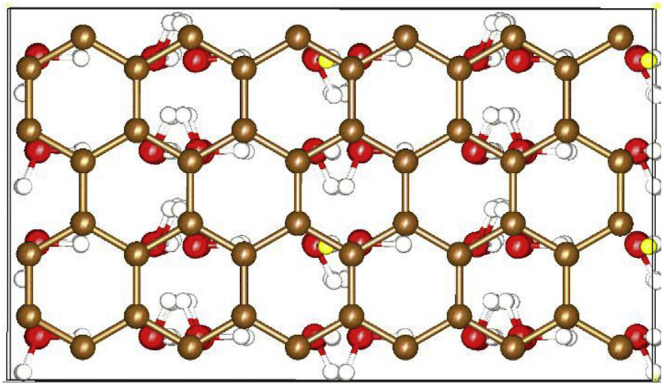

Fig. 8. Bottom view of the (2 × 2) supercell interface ice/graphene. (Red: O atoms, white: H atoms, brown: C atoms. Yellow: H atoms closest to the graphene layer). (For interpretation of the references to colour in this figure legend, the reader is referred to the Web version of this article.)

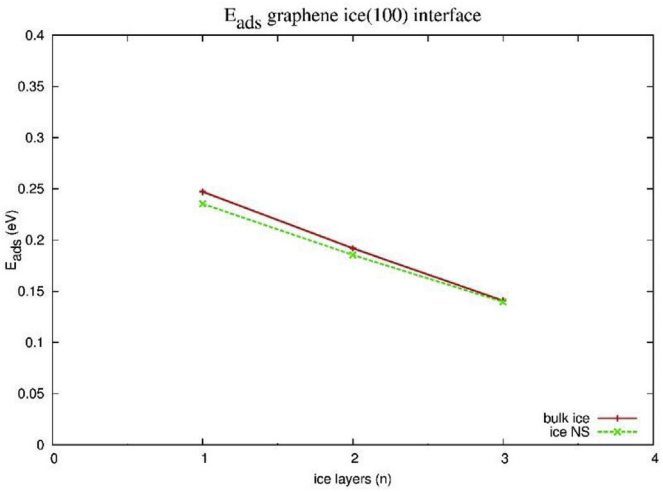

Fig. 9. Relationship between ice thickness (n) and adsorption energy (E_{ads}, eV). $E_{ads}(n) = E_{ads}(1)/n^x$, where $x \cong 0.47$ or 0.51 vs the theoretical value of 0.5.

The overall trend for the two approaches analysed is then shown in Fig. 9, where the relationship between number of ice layers (thickness) and adsorption energy is reported. We are aware of the limits of our modellization, mainly of the fact that we are considering just one ice surface facet and also that the maximum number of ice layers here investigated is three, an amount clearly largely smaller than that of experiments and thus further facets and thickness should be investigated. However such a limitation has been mitigated considering the reported scaling law, thus for better connecting simulations and experiments. Also note that the interface shear strength is predicted to scale as $\tau = K^*(E^*E_{ads})^y$ where E is the modulus, the absorption energy E_{ads} is considered to be proportional to the fracture energy of the rubber-ice interface, K is a dimensional constant of proportionality (a function of the structural size, here fixed, see Ref. [44]) and theoretically -according to fracture mechanics- y = 0.5 [44]. This equation shows a competition between E and E_{ads} for reducing the adhesive shear strength of ice on rubber: the swelling reduces E (see Table 1) whereas the nanocarbon phase increases E (see Table 1) but can reduce E_{ads} and moreover when both swelling and nanocarbon phase are present the competition is not trivial and a clear synergy between these two phases is experimentally emerging. This is summarized in Table 5, where the experiments are compared with the numerical/theoretical predictions, showing a good agreement with y = 0.39.

At the same time, consistent with experiments, we observe that the thicker the ice slab the more icephobic graphene will result. Interestingly, as stated, increasing the thickness of ice leads to a convergence between the two approaches (bulk & NSs) stressing the main role in the formation of the graphene/ice heterostructure played by the very first layers of ice.

On the other hand, to better investigate the icephobicity of graphene we have focused on the binding energy (BE) of ice once forming the interface with graphene. In particular, we have calculated the BE by removing one ice unit (H_2O) from the one- or three-layers of ice and obtained a BE of 0.852 or 0.805 eV, respectively (see Fig. 10). Keeping in mind the fact that the ratio between BE and E_{ads} previously calculated is between 3 (1L) and 6 (3L), we confirm previous theoretical data about the icephobicity of graphene [15] further adding that such icephobicity increases with the thickness of ice.

We want to conclude this section stressing that our modellization does not include the interface formed by ice and CNTs. The reason for such choice is twofold: the first is technical, that is modelling large radius CNTs including their curvatures would imply a sensitive enlargement of the simulation cells, the second motivation stems from previous literature which clearly demonstrated the suitability of graphene layers as precursors of CNTs used in absorption analysis [45].

Considering only the exterior surface of CNTs and regardless their radius, other systems, like molecular hydrogen [46] and oxygen [47], have been found to be quite insensitive in the adsorption process to the layered or tubular nature of such carbonaceous systems, further supporting our choice.

5. Conclusions

Overall, in this work, we report swelling and cross-link density, which can affect the ice adhesion for graphene/carbon nanotubes based elastomeric surfaces. It was found that swollen nanocomposites (i.e. lower cross-link density) have an icephobic surface. Materials with graphene filler show a low level for the interfacial strength. We rationalized such results by means of an atomistic and continuum modellization supporting the observation of a synergy between swelling and

Table 5
Experimental findings of the interface shear strength and of the modulus E (at 50% of strain). The theoretical values of the interface shear strength for the swelled nanocomposites were obtained by the best fit of $\tau = K^*(E^*E_{ads})^y$ with $K = 0.41\ (N/m^2)^{0.61}/(eV)^{0.39}$ and y = 0.39 taking into account the adsorption interface energy with ice $E_{ads} = 0.140eV$ (3L). The theoretical values of the interface shear strength for the NBR samples were obtained by using $\tau = K^*(E^*E_{ads})^y$ with the same previous best fitting values of $0.41\ (N/m^2)^{0.61}/(eV)^{0.39}$, y = 0.39 and rescaling the E_{ads} to the fitting value of 1.2eV considering the experimental moduli of swollen and un-swollen rubber; similarly for non swollen composites we use the fitting value of 1.2eV and their related experimental moduli. The superscripts (*) and (**) indicate the properties after the immersion in Jet A1 Total 20 and isopropyl alcohol, respectively.

Sample (GNPs/CNTs)	$\tau_{Exp.}$ (MPa)	$E_{Exp.}$ (MPa)	$\tau_{Theor.}$ (MPa)
0/0	0.51	0.62	0.50
0/0(*)	0.25	0.49	0.25
0/0(**)	0.26	0.44	0.26
5/0	0.40	1.18	0.40
5/0(*)	0.16	0.96	0.18
5/0(**)	0.16	0.79	0.17
0/5	0.40	0.79	0.50
0/5(*)	0.16	0.69	0.16
0/5(**)	0.17	0.53	0.15
2.5/2.5	0.40	1.03	0.48
2.5/2.5(*)	0.17	0.79	0.17
2.5/2.5(**)	0.17	0.70	0.16

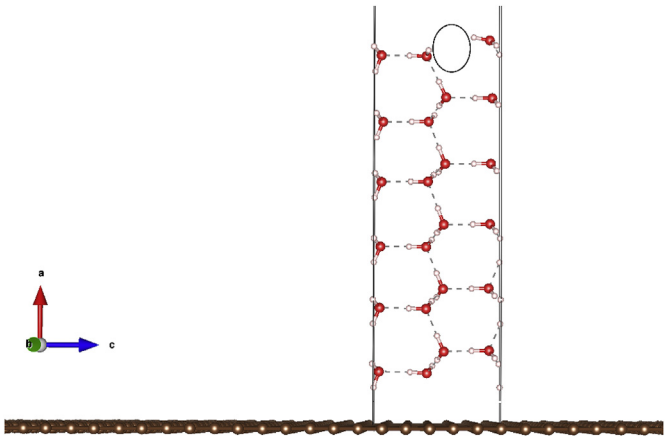

Fig. 10. Optimized structure of the 3L ice/graphene interface after a H_2O ice molecule removal. The position of H_2O ice removed is indicated by the black circle (Red: O atoms, white: H atoms, brown: C atoms. Dashed bonds: H-bonds among water molecules). (For interpretation of the references to colour in this figure legend, the reader is referred to the Web version of this article.)

nanocarbon phase in the icephobic nature of the composite. We pave the exploitation of such results for the realization of rubber nanocomposites that may have applications in rubber based components that need to survive in extreme cold environments.

Acknowledgments

GG wants to thank CINECA [grant number HP10CN7DI0] and acknowledge PRACE for awarding us access to resource Marconi based in Italy at CINECA [Grant number Pra14_3664]. G.G. is similarly grateful to CARIT [grant number FCARITR17FR]" for supporting this research. MALM thanks the support from the MINECO [grant number MAT2016-81138-R]. NMP is supported by the European Commission under the Graphene Flagship Core2 [WP14 "Composites" grant number 785219] and FET Proactive "Neurofibres" [grant number 732344]. NMP is supported by theItalian Ministry of Education, University and Research (MIUR) under the "Departments of Excellence" grant L.232/2016. LV is supported by the European Commission under the Graphene Flagship Core2 [WP14 "Composites" grant number 785219]. LV and GG rea supported by the Italian Ministry of Education, University and Research (MIUR) under the "Departments of Excellence" grant L.232/2016.

Appendix A. Supplementary data

Supplementary data to this article can be found online at https://doi.org/10.1016/j.compositesb.2018.11.095.

References

[1] Mulherin ND, Haehnel RB. Ice engineering: progress in evaluating surface coatings for icing control at corps hydraulic structures. US Army Engineer Research and Development Center; 2003.
[2] Hejazi V, Sobolev K, Nosonovsky M. From superhydrophobicity to icephobicity: forces and interaction analysis. Sci Rep 2013;3:2194–6.
[3] Chen J, Dou R, Cui D, Zhang Q, Zhang Y, Xu F, Zhou X, Wang J, Song Y, Jiang L. Robust prototypical anti-icing coatings with a self-lubricating liquid water layer between ice and substrate. ACS Appl Mater Interfaces 2013;5:4026–30.
[4] Dou R, Chen J, Zhang Y, Wang X, Cui D, Song Y, Jiang L, Wang J. Anti-icing coating with an aqueous lubricating layer. ACS Appl Mater Interfaces 2014;6:6998–7003.
[5] Golovin K, Kobaku SPR, Lee DH, DiLoreto ET, Mabry JM, Tuteja A. Designing durable icephobic surfaces. Sci Adv 2016;2. e1501496–1501512.
[6] Kim P, Wong T-S, Alvarenga J, Kreder MJ, Adorno-Martinez WE, Aizenberg J. Liquid-infused nanostructured surfaces with extreme anti-ice and anti-frost performance. ACS Nano 2012;6:6569–77.
[7] Urata C, Dunderdale GJ, England MW, Hozumi A. Self-lubricating organogels (SLUGs) with exceptional syneresis-induced anti-sticking properties against viscous emulsions and ices. J Mater Chem 2015;3:12626–30.
[8] Wang Y, Yao X, Chen J, He Z, Liu J, Li Q, Wang J, Jiang L. Organogel as durable anti-icing coatings. Sci China Mater 2015;58:559–65.
[9] Zhu L, Xue J, Wang Y, Chen Q, Ding J, Wang Q. Ice-phobic coatings based on silicon-oil-infused polydimethylsiloxane. ACS Appl Mater Interfaces 2013;5:4053–62.
[10] Chaudhury MK, Kim KH. Shear-induced adhesive failure of a rigid slab in contact with a thin confined film. Eur Phys J E Soft Matter 2007;23:175–83.
[11] Flory PJ. Principles of polymer chemistry. Ithaca, New York: Cornell Univ Press; 1953. p. ch11.
[12] Golovin K, Tuteja A. A predictive framework for the design and fabrication of icephobic polymers. Sci Adv 2017;3. e1701617–1701619.
[13] Zhang Y, Rhee KY, Park S-J. Nanodiamond nanocluster-decorated graphene oxide/epoxy nanocomposites with enhanced mechanical behavior and thermal stability. Composites Part B 2017;114:111–20.
[14] Zhang Y, Rhee KY, Hui D, Park S-J. A critical review of nanodiamond based nanocomposites: synthesis, properties and applications. Composites Part B 2018;143:19–27.
[15] Melios C, Giusca CE, Panchal V, Kazakova O. Water on graphene: review of recent progress. 2D Mater 2018;5:022001–18.
[16] Wehling TO, Lichtenstein AI, Katsnelson MI. First-principles studies of water adsorption on graphene: the role of the substrate. Appl Phys Lett 2008;93:202110–3.
[17] Leenarts O, Partoens B, Peeters FM. Water on graphene: hydrophobicity and dipole moment using density functional. Phys Rev B 2009;79:235440–5.
[18] Freitas RRQ, Rivelino R, de Brito Mota F, de Castilho CMC. DFT studies of the interactions of a graphene layer with small water aggregates. J Phys Chem 2011;115:12348–56.
[19] Krause B, Mende M, Pötschke P, Petzold G. Dispersability and particle size distribution of CNTs in an aqueous surfactant dispersion as a function of ultrasonic treatment time. Carbon 2010;48:2746–54.
[20] Ordejòn P, Artacho E, Soler JM. Self–consistent order–N density–functional calculations for very large systems. Phys Rev B 1996;53:R10441–4.
[21] Soler JM, Artacho E, Gale JD, García A, Junquera J, Ordejón P, Sánchez–Portal D. The SIESTA method for ab initio order–N materials simulation. J Phys Condens Matter 2002;14:2745–79.
[22] Dion M, Rydberg H, Schröder E, Langreth DC, Lundqvist BI. Van der Waals density functional for general geometries. Phys Rev Lett 2004;92:246401–2464404.
[23] Lee K, Murray ED, Kong L, Lundqvist BI, Langreth DC. Higher-accuracy van der Waals density functional. Phys Rev B 2010;82:081101–4.
[24] Troullier N, Martins JL. Efficient pseudopotentials for plane–wave calculations. Phys Rev B 1991;43:1993–2006.
[25] Chichagov AV. Information-calculating system on crystal structure data of minerals (MINCRYST). Kristallographiya 1990;35:610–6.
[26] Mellor M. Mechanical properties of polycrystalline ice 217-245, IUTAM symposium copenhagen 1979, physics and mechanics of ice, Editor Per Tryde.
[27] Kraus G. Swelling of filler-reinforced vulcanizates. J Appl Polym Sci 1963;7:861–71.
[28] Boonstra BB. Blow CM, Hepburn C, editors. Rubber technology and manufacture. London: Newnes-Butterworths; 1975.
[29] Flory PJ, Rehner Jr. J. Statistical mechanics of cross-linked polymer networks II swelling. J Chem Phys 1943;11:521–6.
[30] Jung S, Dorrestijn M, Raps D, Das A, Megaridis CM, Poulikakos D. Are superhydrophobic surfaces best for icephobicity? Langmuir 2011;27:3059–66.
[31] Masuda Y, Giorgi G, Yamashita K. DFT study of anatase-derived TiO_2 nanosheets/graphene hybrid materials. Phys Status Solidi B 2014;251:1471–9.
[32] Makov G, Payne MC. Periodic boundary conditions in ab initio calculations. Phys

Rev B 1995;51:4014–22.
[33] Hamann DR. H_2O hydrogen bonding in density-functional theory. Phys Rev B 1997;55:R10157–60.
[34] Perron H, Domain C, Roques J, Drot R, Simoni E, Catalette H. Optimisation of accurate rutile TiO_2 (110), (100), (101) and (001) surface models from periodic DFT calculations. Theor Chem Acc 2007;117:565–74.
[35] Giorgi G, Fujisawa J-I, Segawa H, Yamashita K. Unraveling the adsorption mechanism of aromatic and aliphatic diols on the TiO_2 surface: a density functional theory analysis. Phys Chem Chem Phys 2013;15:9761–7.
[36] Giorgi G, Yamashita K, Segawa H. First-Principles investigation of the Lewis acid-base adduct formation at the methylammonium lead iodide surface. Phys Chem Chem Phys 2018. https://doi.org/10.1039/C8CP01019F.
[37] Ma J, Michaelides A, Alfè D, Schimka L, Kresse G, Wang E. Adsorption and diffusion of water on graphene from first principles. Phys Rev B 2011;84:033402–4.
[38] Boys SF, Bernardi F. The calculation of small molecular interactions by the differences of separate total energies Some procedures with reduced errors. Mol Phys 1970;19:553–66.
[39] Chen J, Schusteritsch G, Pickard CJ, Salzmann CG, Michaelides A. Two dimensional ice from first principles: structures and phase transitions. Phys Rev Lett 2016;116:025501–6.
[40] Xu K, Cao P, Heath JR. Graphene visualizes the first water adlayers on mica at ambient conditions. Science 2010;329:1188–91.
[41] Algara-Siller G, Lehtinen O, Wang FC, Nair RR, Kaiser U, Wu HA, Geim AK, Grigorieva IV. Square ice in graphene nanocapillaries. Nature (London) 2015;519:443–5.
[42] Li Q, Song J, Besenbacher F, Dong M. Two-dimensional material confined water. Acc Chem Res 2015;48:119–27.
[43] Carpinteri A, Pugno N. Are the scaling laws on strength of solids related to mechanics or to geometry? Nat Mater 2005;4:421–3.
[44] Pugno N, Carpinteri A. Tubular adhesive joints under axial load. J Appl Mech 2003;70:832–9.
[45] Ishii A, Yamamoto M, Asano H, Fujiwara K. DFT calculation for adatom adsorption on graphene sheet as a prototype of carbon nano tube functionalization. J Phys: Conf Ser 2018;100. 052087–052084.
[46] Henwood D, Carey JD. Molecular physisorption on graphene and carbon nanotubes: a comparative ab initio study. Mol Simulat 2008;34:1019–23.
[47] Giannozzi P, Car R, Scoles AG. Oxygen adsorption on graphite and nanotubes. J Chem Phys 2003;118:1003–6.

Synergistic icephobic behaviour of swollen nitrile butadiene rubber graphene and/or carbon nanotube composites

Supplementary Material

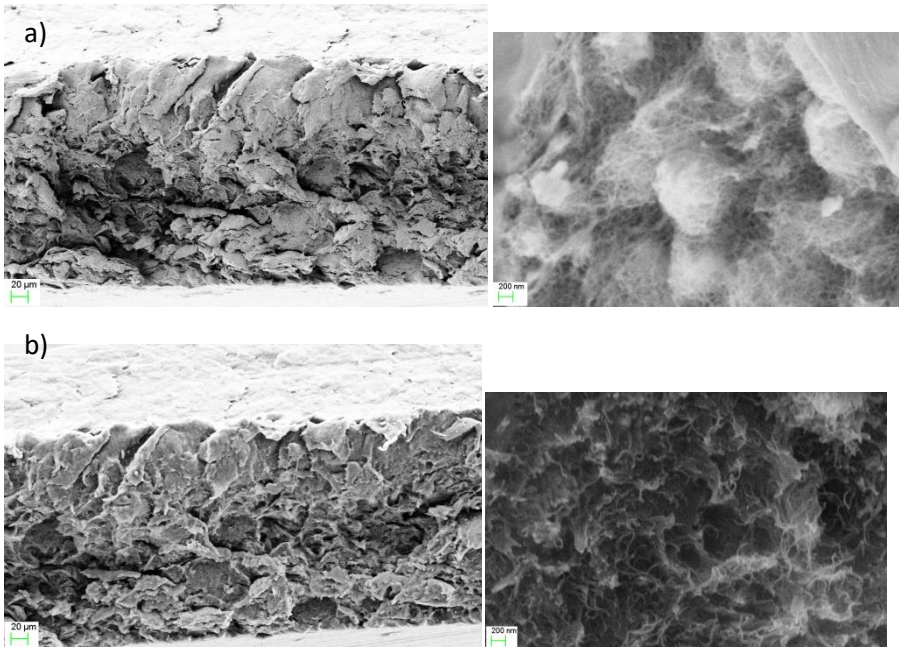

Figure S1. FESEM images at different magnifications of the cross section of the (a) 0/5 and (b) 2.5/2.5 nanocomposites.